Sánchez Tovar, R.; Montañés, M.; Garcia-Anton, J.; Guenbour, A. (2010). Effect of Temperature on Galvanic Corrosion of Non-Welded/Welded AISI 316L Stainless Steel in H3PO4. ECS Transactions. 25(37):63-81. https://doi.org/10.1149/1.3407548

Effect of Temperature on Galvanic Corrosion of Non-Welded/Welded AISI 316L Stainless Steel in H_3PO_4

R. Sánchez-Tovar[a], M.T. Montañés[a], J. García-Antón[a*], A. Guenbour[b]

[a] Department of Nuclear and Chemical Engineering, Polytechnic University of Valencia, Valencia 46022, Spain
[b] Laboratory Corrosion-Electrochimie, Faculty of Science, University Mohammed V-Agdal, Rabat, Morocco

[*]Corresponding author. Tel.: +34-96-3877632; fax: +34-96-3877639;
e-mail address: jgarciaa@iqn.upv.es

Abstract

Galvanic corrosion of non-welded/welded AISI 316L SS at different temperatures (25 ºC to 60 ºC) at a Reynolds number of 1456 in phosphoric acid media has been studied by means of different electrochemical techniques: polarization curves (by the mixed potential theory) and zero resistance ammeter (ZRA) measurements. Imposed potential measurements provide more active predicted coupled potentials and higher galvanic current densities than those obtained using ZRA measurements. Polarization curves show that the anode of the pair is the non-welded AISI 316L. Galvanic current density values obtained from polarization curves increase with temperature. ZRA tests present the highest i_G values at 60 ºC, however, the values are very close to zero for all the temperatures studied. This is in agreement with the low value of the compatibility limit and of the parameter which evaluate the galvanic phenomenon important. Both techniques present the most positive potentials at the highest temperature.

Introduction

Austenitic stainless steels, as well as their welded forms, are widely used in the phosphoric acid industry, for instance, in piping systems. This is due to the fact that they have excellent corrosion and heat resistance with good mechanical properties over a wide range of temperatures (1). In particular, AISI 316L stainless steel (SS) is used for its good mechanical properties and corrosion resistance (2). Therefore, it would be suitable to store and transport phosphoric acid at different temperatures. Owing to their low carbon content, AISI 316L SS are appropriate when high temperature treatment is applied (such as welding) and consequently, corrosion along the grain boundaries could take place (3). Welding introduces metallurgical changes and residual stresses in materials, diminishing their corrosion resistance. In fact, welds are recognized as zones which are particularly sensitive to corrosion (4). Furthermore, the use of welded materials could result in the formation of galvanic pairs that may accelerate the corrosion processes and temperature enhances these corrosion problems (5, 6). On the other hand, the effect of fluid flow has

been considered as one of the major problems in the corrosion field since it also increases corrosion rates (7).

Plasma arc welding (PAW) is an innovative arc welding process (8) similar to gas tungsten arc welding (GTAW). The key difference from GTAW is that in PAW the plasma arc can be separated from the shielding gas envelope. PAW represents an advance over GTAW, due to its greater energy concentration, deep and narrow penetration achievement and greater arc stability. Micro-plasma arc welding (MPAW) is a variation of the PAW process and uses intensities lower than 15 A. Several authors have studied the MPAW technology (9-12). On the other hand, there is no research related to AISI 316L stainless steels MPAW that takes into consideration the galvanic corrosion, especially in phosphoric acid solutions.

The use of polarization curves has become widespread during the last years, due to its versatility (13). However, the application of a zero-resistance ammeter (ZRA) as an electrochemical measurement technique is gaining importance because it can be used without disturbing the system under investigation. ZRA permits to register potential and current fluctuations in the corroding electrodes during a corrosion process (14).

Many studies have focused on the influence of temperature on corrosion in phosphoric acid media, such as, corrosion of steel at different acid concentrations (15), corrosion behaviour of stainless steels in H_3PO_4 polluted by sulphide ions (16) and corrosion behaviour of graphite and stainless steel in polluted phosphoric acid (17). However, these studies are based on weight lost and polarization curves measurements. The objective of this work is to study the effect of temperature on the galvanic corrosion of the non-welded/welded AISI 316L SS pair at a Reynolds number (Re) of 1456 by means of different electrochemical measurements. Galvanic corrosion has been studied under open circuit conditions using a zero-resistance ammeter (ZRA). The results obtained have been compared with the results estimated from the polarization curves according to the mixed potential theory (imposed potential measurements).

Experimental

Materials

The materials studied were rings 14 mm and 16 mm in inner and external diameter, respectively, and 20 mm in length, made of AISI 316L SS (16.957% Cr, 10.171% Ni, 1.337% Mn, 2.298% Mo, 0.004% S, 0.368% Si, 0.030% P, 0.022% C, Bal.% Fe) and micro-plasma arc welded AISI 316L SS. The base material was always AISI 316L SS and it was welded with AISI 316L filler alloy (18.160% Cr, 12.100% Ni, 1.860% Mn, 2.540% Mo, 0.007% S, 0.760% Si, 0.018% P, 0.010% C, 0.080% Cu, 0.050% N, Bal.% Fe) and with baking gas (99.9% Ar). Welding was performed from two rings 10 mm in length. The composition of the filler alloy is more noble than that of the base material. In spite of this, compositions of both the base and the filler alloy are very similar in order to avoid future galvanic problems. The argon backing gas was used to protect the inner surface of the materials while the welding process was being carried out (18). The flow rate of this shielding gas was 2.5 L/min. The welding process presented two steps (step one: current = 11.3 A, voltage = 20 V, welding speed = 2.6 mm/s; and step two: current =

13 A, voltage = 20 V, welding speed = 2.6 mm/s). The flow rate of the plasma gas was 6.5 L/min. Figure 1 shows a photograph of the non-welded and the welded AISI 316L SS rings.

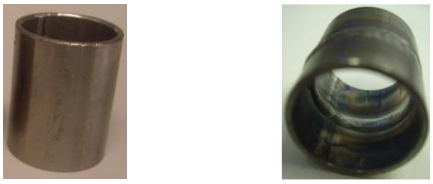

Non-welded AISI 316L Welded AISI 316L

Figure 1. Photographs of the different materials studied.

Materials were examined by light microscopy (LM) to reveal their microstructure and compare it with the microstructure of the base alloy, to estimate possible microstructural variations produced during the micro-plasma arc welding procedure. To this end, each material was cut lengthwise and covered in resin; afterwards, the samples were wet abraded from 220 silicon carbide (SiC) grit to 4000 SiC grit. Then, they were polished with 1 and 0.3 micron alumina and were rinsed with distilled water and ethanol. Once the samples were polished, metallographic etching was carried out according to ASM International (19). The etchant composition consisted of 10 mL of nitric acid, 10 mL of acetic acid, 15 mL of hydrochloric acid and 5 mL of glycerine. Samples were immersed in the etching solution during 90 seconds and then rinsed with distilled water and ethanol.

Hydrodynamic circuit

Figure 2 shows the hydrodynamic circuit, based on one designed in a previous work (20), used to study dynamic corrosion. It consists of a centrifugal pump, a flow-meter, a thermostat to regulate the solution temperature, a test section (where the rings are assessed), a valve to drain the system and several glass devices: for the reference electrode (Ag/AgCl, 3M KCl), for the auxiliary electrode (Pt), for the gas output, to introduce the solution into the flow circuit and to bubble an inert gas. Silicone flexible tubes were used to assemble the different elements. Fully developed flow was assured using a 90-cm-long Teflon rigid tube of the same inner diameter as the test rings upstream of the test section.

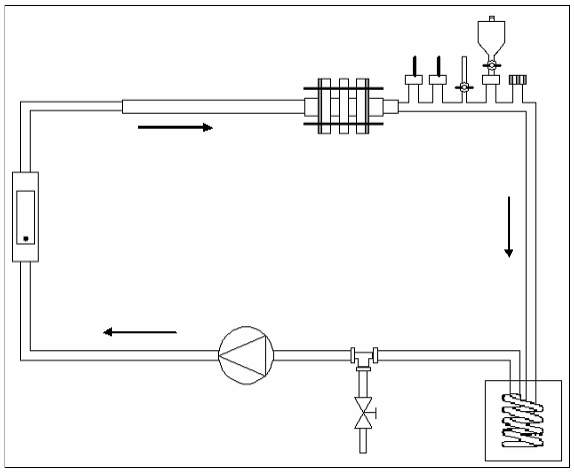

Figure 2. Scheme of the hydrodynamic circuit used in the study.

Operating conditions

Materials were tested in a 5.5 M H_3PO_4 solution (40 wt. % H_3PO_4, typical in phosphoric acid industries). The experiments were carried out at a Reynolds number (Re) of 1456 at 25 ºC, 40 ºC and 60 ºC in order to study the influence of temperature on the galvanic corrosion. An area of 8.8 cm^2 was exposed to the solution.

Electrochemical tests

Two different electrochemical techniques were used in the corrosion studies: polarization curves and zero-resistance ammeter measurements.

Polarization curves. Cyclic potentiodynamic curves of the materials were obtained according to the ASTM G-61 (21) using a potentiostat. Before each test, the rings were degreased with ethanol and dried with air. Dissolved oxygen was removed from the solution by bubbling nitrogen during 60 minutes. Furthermore, nitrogen was bubbled when the solution was inside the hydrodynamic circuit during 10 minutes thanks to the glass device located in the hydraulic circuit for this purpose. Then, the hydrodynamic circuit was completely closed to keep these conditions. All the tests have been repeated at least three times in order to verify reproducibility.

Before each polarization experiment, the open circuit potential was recorded for one hour; the open circuit potential value (OCP) reported here is the arithmetic mean of the last five minute values, when a fully developed flow is reached (22). After the OCP test, the potential was reduced progressively to –400 $mV_{Ag/AgCl}$; then, the working electrode potential was scanned from –400 $mV_{Ag/AgCl}$ to the anodic direction until the current density reached 0.2 mA/cm^2, using a scan rate of 1 mV/s. Figure 3 shows a schematic diagram of the physical arrangement of the electrodes in the test section.

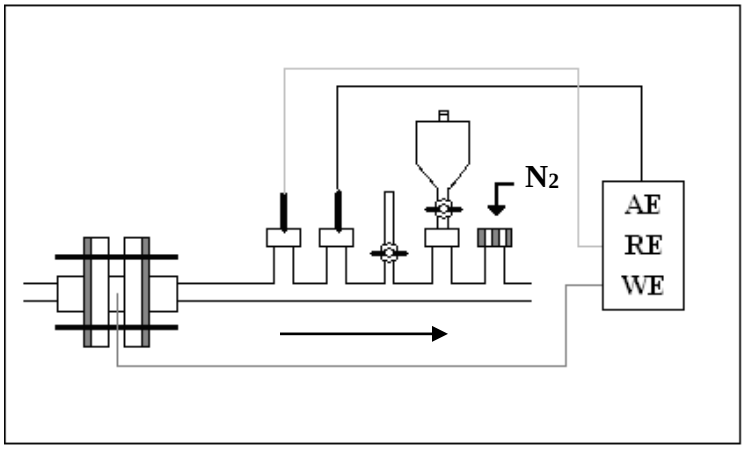

Figure 3. Schematic diagram of the physical arrangement of the electrodes in the test section to carry out polarization curves. AE: auxiliary electrode. RE: reference electrode. WE: working electrode.

The galvanic corrosion between the non-welded AISI 316L SS and the welded AISI 316L SS was evaluated from the polarization curves, by superimposing the potentiodynamic curves of both materials. The predicted coupled potential (E_{coup}) and the

galvanic current density (i_{coup}) of the pair were estimated from the intersection point of the anodic curve of one alloy with the cathodic curve of the other one, according to the mixed potential theory (23).

Zero-resistance ammeter (ZRA) measurements. The galvanic current density (i_G) and the galvanic potential (E_G) established between the pair were measured with a ZRA every 0.5 s during 8 h. The current sign was positive when the direction of the electrons was from working electrode 1 (WE1) to WE2; thus, WE1 was corroding. Current values were negative when the electrons flowed in the opposite direction, that is, the WE2 was corroding. The tests were designed with the non-welded AISI 316L as WE1 and the welded AISI 316L as WE2. Figure 4 shows a schematic diagram of the physical arrangement of the electrodes in the test section.

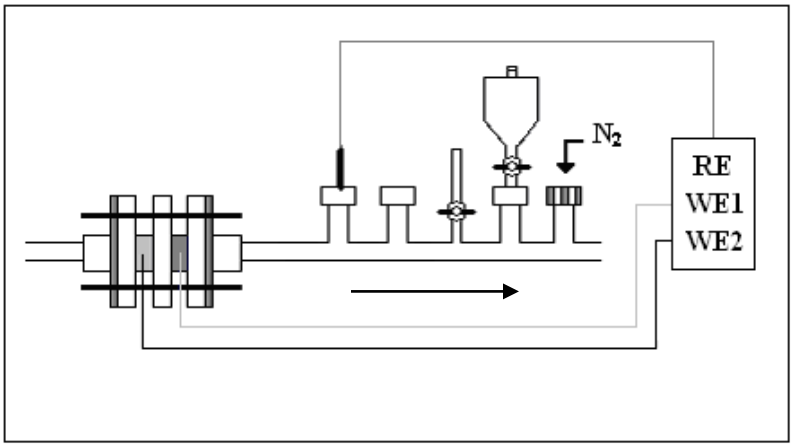

Figure 4. Schematic diagram of the physical arrangement of the electrodes in the test section to carry out ZRA measurements. RE: reference electrode. WE1: working electrode 1. WE2: working electrode 2.

Results and discussion

Microstructural examination

To analyse the effect that welding causes in the microstructure of the AISI 316L SS and, consequently, on the galvanic corrosion of the non-welded/welded AISI 316L SS a microstructural analysis of the materials was performed. Figure 5a shows the microstructure of the non-welded AISI 316L SS after etching examined by Light microscopy (LM). This is a single-phase austenitic microstructure with equiaxed grains. The base zone of the welded alloy (Figure 5b) also shows this austenitic microstructure. On the other hand, Heat affected zone (HAZ) microstructure can be observed in Figure 5c. The microstructure of this zone is characterized by an increase in grain size due to the fact that there is not transformation point at temperatures higher than room temperature (24). Figure 5d shows the microstructure of the weld zone corresponding to the welded AISI 316L SS. The weld zone has columnar grains where delta-ferrite can be found. Alloys with especially low carbon contents (such as AISI 316L SS), to minimize susceptibility to sensitization during welding, present a greater tendency toward delta-

ferrite stabilization (25). The microstructure of delta-ferrite occurs in vermicular form. Vermicular morphology is typical of welds that solidify ferrite, followed by a subsequent formation of austenite involving the grains of ferrite until complete solidification. Microstructures shown in Figure 5 do not present carbide precipitation, since AISI 316L SS is a stainless steel with low carbon content.

a. Non-welded AISI 316L 200x **b.** Welded AISI 316L (base zone) 100x

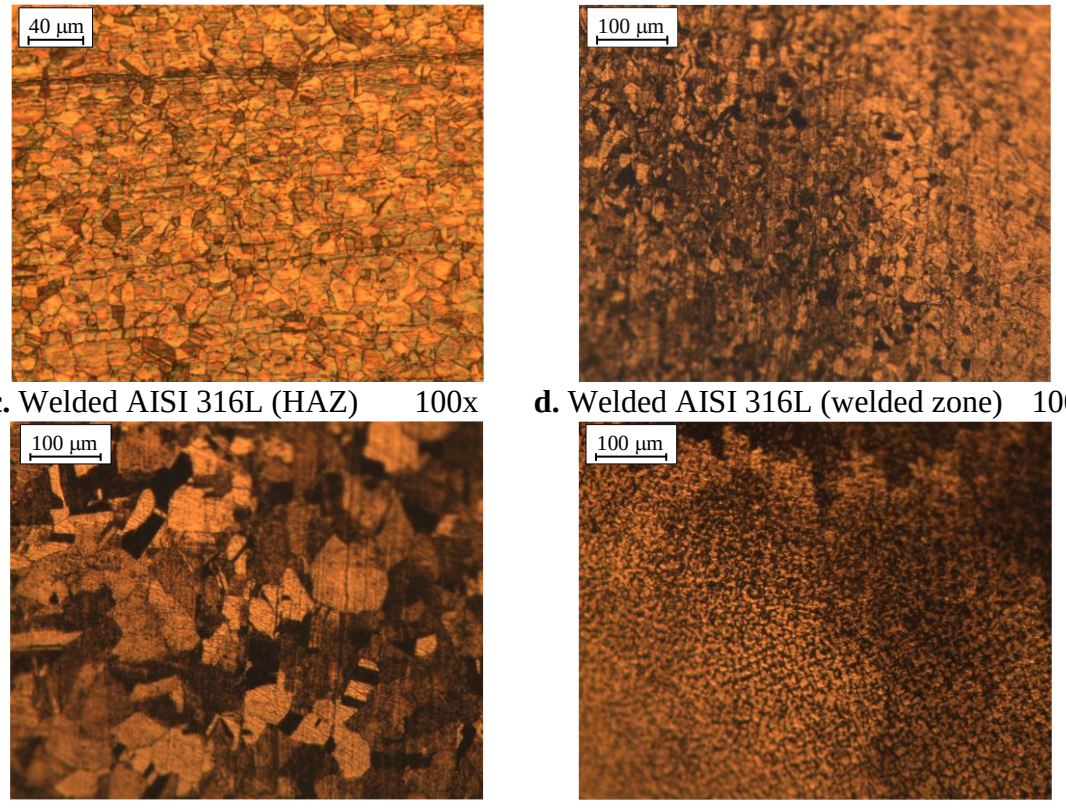

c. Welded AISI 316L (HAZ) 100x **d.** Welded AISI 316L (welded zone) 100x

Figure 5. Microstructure of the non-welded AISI 316L SS (a) and the welded AISI 316L SS corresponding to the base zone (b), the HAZ (c) and the welded zone (d) examined by LM.

Potentiodynamic curves

Influence of temperature on the individual corrosion of the materials. Figure 6 shows the cyclic potentiodynamic curves obtained for the non-welded and the welded AISI 316L SS.

a. Non-welded AISI 316L SS **b.** Welded AISI 316L SS

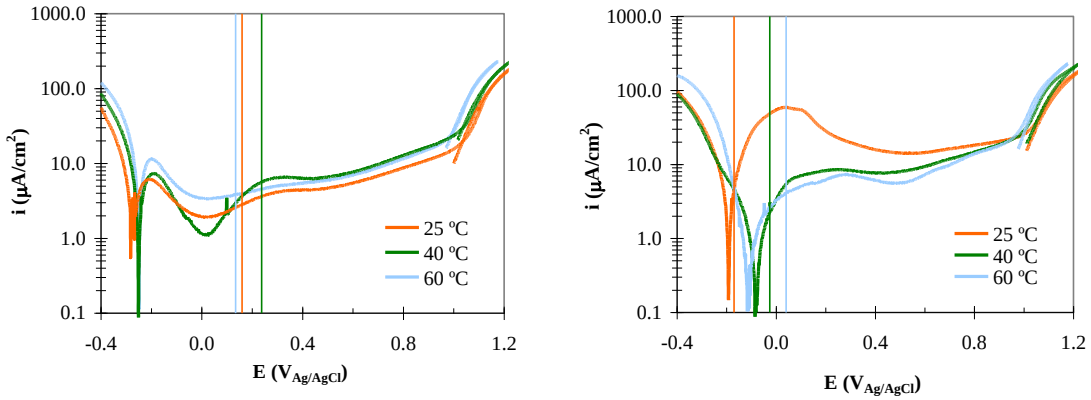

Figure 6. Cyclic polarization curves of the non-welded (a) and welded (b) AISI 316L SS in 5.5 M H_3PO_4 solutions at a Reynolds number of 1456 and different temperatures. The vertical lines indicate the OCP value for each temperature analysed.

Polarization curves shown in Figure 6 are typical of passivable materials. Moreover, the OCP values obtained at the different temperatures indicate that both the non-welded and the welded AISI 316L SS passivate spontaneously. Temperature seems to shift the corrosion potentials to more noble values whereas critical potentials shift to more active values with temperature. The critical potential indicates the breakdown of the passive film (26). Owing to the fact that temperature accelerates the corrosion rate, the breakdown of the passive film can occur at more negative potentials. On the one hand, Figure 6a shows a slightly increase in the passivation current densities as temperatures increases for the non-welded AISI 316L SS. On the other hand, Figure 6b demonstrates that the effect on the passivation current density of the welded material is the opposite.

Cyclic polarization curves do not show hysteresis loop; that fact indicates that AISI 316L SS undergoes uniform corrosion in phosphoric acid media.

Mixed Potential Theory. Figure 7 shows the superimposing of the cyclic polarization curves of the non-welded/welded AISI 316L SS galvanic pair, the predicted coupled potential (E_{coup}) and the galvanic current density (i_{coup}) at the different temperatures studied.

a. T = 25 ºC

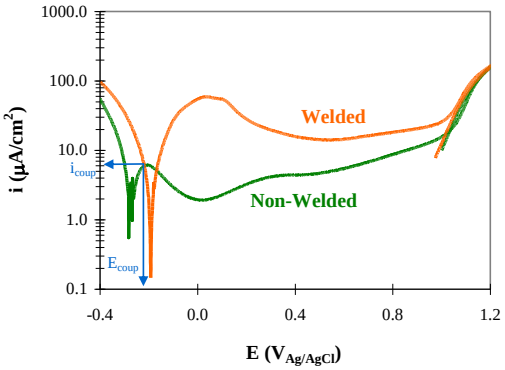

b. T = 40 ºC

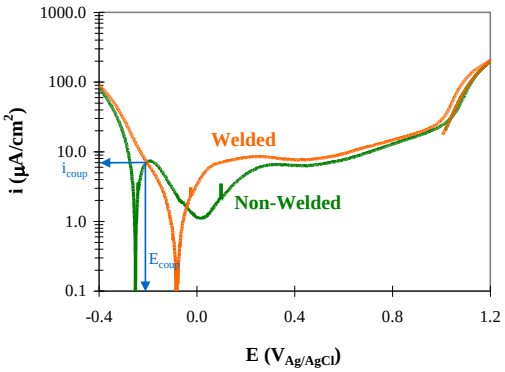

c. T = 60 ºC

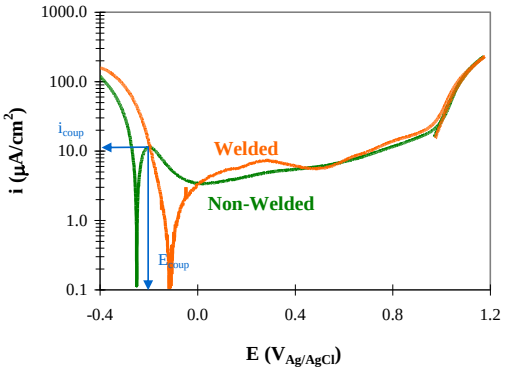

Figure 7. Potentiodynamic curves of the non-welded/welded AISI 316L SS galvanic pair in 5.5 M H_3PO_4 solutions at a Reynolds number of 1456 and at different temperatures.

Figure 7 demonstrates that welding modifies the characteristics of the materials, increasing the passivation current density. However, this difference is lower as temperature increases. In all the cases, the corrosion potential of the non-welded AISI 316L SS is more active than that obtained for the welded materials; therefore, polarization curves indicate that at all the temperatures analysed the non-welded AISI 316L is the anode of the pair.

Galvanic corrosion evaluation. Cyclic polarization curves from Figure 7 indicate that the anode of the pair is the non-welded AISI 316L SS; therefore, it is corroding while the welded material remains protected. This fact could be due to the higher Cr, Ni and Mo contents of the materials welded with filler alloy which generate a better passivation film. In order to study the differences between the corrosion process of the uncoupled non-welded AISI 316L SS and the galvanic corrosion that occurs due to the pair formation with the welded AISI 316L SS, parameters from potentiodynamic curves were obtained. Then the results were compared with the parameters achieved from the mixed potential theory. Corrosion potentials (E_{corr}) and corrosion current densities (i_{corr}) were obtained for the non-welded AISI 316L SS at the different temperatures studied (Table I). For this material, i_{corr} values were determined from the cathodic branch of the polarization curves since the anodic branch do not show a clear linear tendency (27-29). In all the cases, the extrapolation started over about 50 mV away from E_{corr} and the same range of potential values has been always used (30).

TABLE I. Corrosion current densities and corrosion potentials of non-welded AISI 316L SS in 5.5 M H_3PO_4 solutions at Re = 1456 and at different temperatures.

	25 ºC	**40 ºC**	**60 ºC**
i_{corr} ($\mu A/cm^2$)	4.9	6.4	10.2
E_{corr} ($mV_{Ag/AgCl}$)	-282	-251	-250

Table I shows that temperature increases corrosion current densities, since it enhances corrosion rate (5, 6). On the other hand, corrosion potentials shift to more positive when temperature changes to 25 ºC to 40 ºC; then their values seem to remain constant.

Table II shows the predicted coupled potential and the galvanic current density obtained according to the mixed potential theory (23), as well as the differences between corrosion potentials of the cathodic and the anodic member of the pair (E_C-E_A) and the ratio i_{couple}/i_{corr}, where i_{corr} is the corrosion current density of the uncoupled anodic member.

TABLE II. Parameters obtained from the superimposing of the polarization curves of the non-welded/welded AISI 316L SS pair in 5.5 M H_3PO_4 solutions at Re = 1456 and at different temperatures.

	25 ºC	**40 ºC**	**60 ºC**
i_{coup} ($\mu A/cm^2$)	5.9	7.0	11.7
E_{coup} ($mV_{Ag/AgCl}$)	-218	-203	-195
E_C - E_A (mV)	90	165	131
i_{coup}/i_{corr}	1.20	1.10	1.15

Table II shows that predicted coupled potentials have the same tendency as the corresponding potentials to the uncoupled non-welded material; they shift to more noble values as temperature increases. Minimal differences of 100-130 mV between the corrosion potential of the cathode and the anode of the pair (E_C-E_A) are necessary to consider the galvanic effect significant (31). Table II shows that, at all the temperatures studied, the (E_C-E_A) values are lower or close to 130 mV; therefore, the galvanic effect on the non-welded/welded AISI 316L SS pair seems not to be significant.

On the other hand, galvanic current density values increase with temperature. According to Mansfeld and Kendel (32), the relative increase in the corrosion rate of the anode of the galvanic pair could be expressed by the ratio i_{couple}/i_{corr}, where i_{corr} is the corrosion current density of the uncoupled anode. The magnitude of this ratio may be used as a guide to reflect the severity of the galvanic effect, and it was suggested that a i_{couple}/i_{corr} value lower than 5 implies compatibility of the members in a galvanic pair (33). Table II shows that the i_{couple}/i_{corr} values are lower than 2 in all the cases analysed; therefore, it can be concluded that the galvanic corrosion of the non-welded/welded AISI 316L SS pair in a 5.5 M H_3PO_4 solutions is not severe.

In general, the rate of most reactions increases with temperature following Arrhenius equation (34). In the case of electrochemical reactions, temperature favours the kinetics of corrosion reactions and, more specifically, the anodic dissolution of the metal (35-37). The activation energy of the corrosion process can be obtained from Arrhenius-type plots according to the following equation:

$$i_{corr} = A \cdot e^{-\frac{E_a}{R \cdot T}} \qquad [1]$$

where E_a is the molar activation energy of the process (J/mol), R is the universal gas constant (8.314 J/(mol·K)), T is the temperature (K) and A is a constant. Taking the logarithm of the Arrhenius equation yields:

$$\mathrm{Log}(i_{corr}) = \mathrm{Log}(A) - \frac{E_a}{2.303 \cdot R \cdot T} \qquad [2]$$

Therefore, the values of activation energy of a corrosion process can be determined from the slope of Log(i_{corr}) versus 1/T plots (38).

Corrosion current density values of the non welded AISI 316L SS (Tables I), as well as the galvanic current density of the pair (Table II), have been plotted according to Equation 2 in Figure 8. The molar activation energy of an electrochemical process refers to the energy level that must be overcome by one electron in the exchange through the electrode/electrolyte interphase. In this way, low E_a values indicate high corrosion rates. Moreover, Arrhenius equation indicates that the greater the dependence of the corrosion rate on temperature, the higher the E_a values (34). Figure 8 also shows the linear plots encountered for the uncoupled and coupled non-welded AISI 316L SS. Due to the proportionality between the slope of Equation 5 and the activation energy value, the E_a tendency will be discussed in terms of the slope values obtained.

As it can be observed in Figure 8, both experimental values of the corrosion current density of the non-welded AISI 316L SS and of the galvanic current density of the pair fit well the Arrhenius plot. Furthermore, the E_a value obtained for the uncoupled non-welded AISI 316L SS is higher than the calculated from the mixed potential theory (MPT) for the galvanic pair. This fact could be expected because the corrosion rate of the non-welded AISI 316L SS increases due to the galvanic effect.

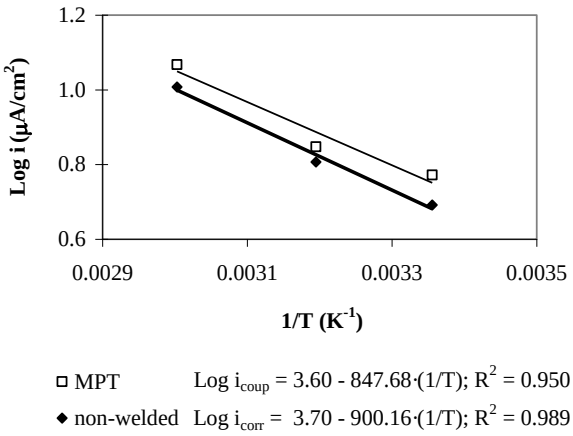

Figure 8. Dependence of the corrosion current densities of the non-welded AISI 316L SS and coupled current densities of the pair (obtained from the mixed potential theory, MPT) on the temperature according to Arrhenius plot.

ZRA measurements

Figure 9 shows the galvanic current density (i_G) and the galvanic potential (E_G) profiles obtained during 8 h for the non-welded/welded AISI 316L SS pair in H_3PO_4 media at a Re of 1456 and at all the temperatures studied by means of ZRA measurements.

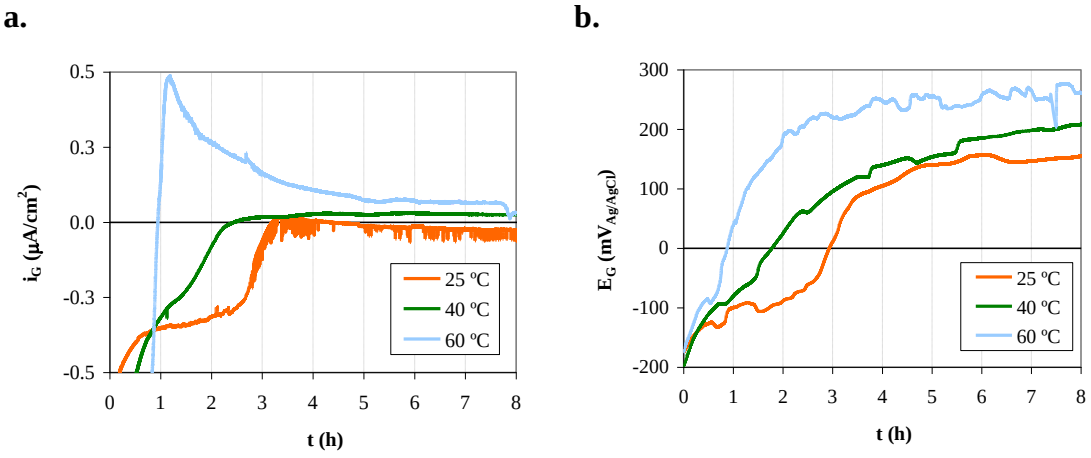

Figure 9. Galvanic current density (a) and potential profiles (b) of the non-welded/welded AISI 316L SS pair at a Re of 1456 at the different temperatures analysed in 5.5 M H_3PO_4 solutions.

Figure 9 shows that galvanic current densities are negative during the first hours of the tests. In particular, during the first hour, the two first hours and along the three first hours

of the tests carried out at 25 ºC, 40 ºC and 60 ºC, respectively. Therefore, during these first hours, the anode of the pair is the welded AISI 316L SS. The general tendency of the galvanic current density is to diminish with time (that is; the values tends to zero). The trend to values close to zero is favoured by temperature. This fact could be explained since temperature enhances corrosion rates (5, 6) consequently; passivation of the welded AISI 316L SS occurs earlier. Once passivation of the welded material takes place, there is a change in the polarity for the higher temperatures analysed which means that the non-welded AISI 316L SS is corroding. Moreover, at 40 ºC i_G values remain positive but near to zero. At 60 ºC, as time passes, galvanic current density tends to decrease with time and beyond the sixth hour, to stabilize. The decrease in galvanic current density is attributed to metal passivation due to the formation of a protective film which grows with time (39). On the other hand, at 25 ºC galvanic current density values change to positive values during the forth hour; then i_G becomes negative but remains practically equal to zero.

On the other hand, the general tendency of the galvanic potential profiles is to become more positive with time. Furthermore, the values seem to stabilize from the sixth hour of the tests; beyond that time, galvanic current density profiles become stable. The most noble galvanic potentials corresponds to the highest temperature studied (60 ºC) and the most active to the lowest one (25 ºC).

Figure 9 also shows that the galvanic current density and the galvanic potential profiles registered present very few individual events; this is a characteristic of uniform corrosion processes (40). Moreover, the most remarkable characteristic of uniform corrosion processes is to present low amplitudes potential and current signals (14), like those registered by the non-welded/welded AISI 316L SS pair.

Polarization curves vs ZRA measurements

Table III shows a comparison between the parameters obtained by the mixed potential theory (MPT) and the ZRA measurements at the different temperatures analysed. Due to the fact that the registers of the i_G and E_G values seem to stabilize from the sixth hour of the ZRA tests, table III shows the mean value of the three last hours of the tests (from sixth to eight hour) corresponding to these parameters.

TABLE III. Comparison between parameters obtained by the application of the mixed potential theory and by means of the ZRA measurements of the non-welded (nw)/welded (w) AISI 316L SS pair in 5.5 M H_3PO_4 solutions at Re = 1456 and at different temperatures.

	25 ºC		**40 ºC**		**60 ºC**	
	MPT	**ZRA**	**MPT**	**ZRA**	**MPT**	**ZRA**
Anode	nw	w	nw	nw	nw	nw
i ($\mu A/cm^2$)	5.92	0.02	7.04	0.03	11.69	0.07
E ($mV_{Ag/AgCl}$)	-218	150	-203	188	-195	255

Results show that the imposed potential measurements provide more active predicted coupled potentials and higher galvanic current densities than those obtained using ZRA measurements. This could be explained due to the formation of a passive film during the open circuit tests, whereas this passive film is modified at the beginning of the polarization measurements owing to the applied potential (41, 42). Galvanic current density values obtained from the polarization curves increase with temperature. Regarding the ZRA tests, the highest i_G are obtained at 60 ºC, however, the values are very close to zero for all the temperatures studied. This is in agreement with the E_C-E_A obtained values (which are low or close to the minimum value necessary to consider the galvanic phenomenon important), together with the low i_{coup}/i_{corr} values (in all the cases lower than 5).

Both techniques agree that AISI 316L stainless steels undergo uniform corrosion in phosphoric acid medium, since no hysteresis loop was observed in the potentiodynamic tests and galvanic current density and potential profiles do not register individual events in the ZRA registers.

ZRA measurements alloy to study the corrosion processes by the registration of the galvanic current density and the galvanic potential without disturbing the system. Furthermore, ZRA tests make possible to obtain the evolution of the parameters registered with time. On the other hand, polarization curves are a suitable electrochemical measurement when fast information wants to be achieved. Moreover, polarization curves provide information from both the uncoupled materials and the galvanic pair; therefore, this is a versatile technique.

Conclusions

The effect of temperature on the galvanic corrosion of the non-welded/welded AISI 316L SS pair in H_3PO_4 solutions at a Re of 1456 has been studied by means of two different electrochemical measurements: polarization curves and ZRA tests. In this way results show that i_{coup} values increase with temperature. ZRA tests present the highest i_G values at 60 ºC, however, the values are very close to zero for all the temperatures studied. This is in agreement with the low E_C-E_A and i_{coup}/i_{corr} obtained values. The most positive E_{coup} and E_G values are obtained at the highest temperature studied (60 ºC).

The imposed potential measurements provide more active predicted coupled potentials and higher galvanic current densities than those obtained using ZRA measurements.

Both techniques agree that AISI 316L stainless steels undergo uniform corrosion in phosphoric acid medium.

Polarization curves and ZRA measurements provide useful and complementary information to study the galvanic corrosion processes. Therefore, the use of both techniques is recommendable in the galvanic corrosion analyses to compare the results obtained.

Acknowledgments

The authors would like to express their gratitude to the Spanish MAEC (PCI Mediterráneo C/018046/08).

References

1. A. I. Almarshad and D. Jamal, *J. Appl. Electrochem.*, **34**, 67 (2004).
2. J. Oñoro, *Int. J. Pres. Ves. Pip.*, **86**, 656 (2009).
3. R. W. K. Honeycombe and H. K. D. H. Bhadeshia, *Steels. Microstructure and properties*, p. 264, Butterworth Heinemann, Great Britain (2006).
4. M. Dadfar, M. H. Fathi, F. Karimzadeh, M. R. Dadfar and A. Saatchi, *Mat. Lett.*, **61**, 2343 (2007).
5. P. Becker, *Phosphates and phosphoric acid. Raw materials, technology, and economics of the wet process*, p. 574, Marcel Dekker, New York (1989).
6. A. Guenbour, H. Iken, N. Kebkab, A. Bellaouchou, R. Boulif and A. Benbachir, *Appl. Surf. Sci.*, **252**, 8710 (2006).
7. T. Y. Chen, A. A. Moccari and D. D. Macdonald, *Corrosion*, **48**, 239 (1992).
8. J. Niu, W. Guo, M. Guo and S. Lu, *Vacuum*, **65**, 263 (2002).
9. F. Javidrad and R. Rahmati, *Mater. Design*, **30**, 1524 (2009).
10. F. Javidrad, H. Farghadani and A. Asgharzadeh, *J. Sci. Eng.*, **31**, 67 (2008).
11. F. Karimzadeh, A. Ebnonnasir and A. Foroughi, *Mater. Sci. Eng. A*, **432**, 184 (2006).
12. F. Karimzadeh, M. Salehi, A. Saatchi and M. Meratian, *Mater. Manuf. Process.*, **20**, 205 (2005).
13. E. Blasco-Tamarit, A. Igual-Muñoz, J. García-Antón and D. García-García, *Corros. Sci.*, **50**, 3590 (2008).
14. J. R. Kearns, D. A. Eden, M. R. Yaffe, J. V. Fahey, D. L. Reichert and D. C. Silverman., ASTM Standardization of Electrochemical Noise Measurement ASTM STP 1277 (1996).
15. M. Benabdellah and B. Hammouti, *Appl. Surf. Sci.*, **252**, 1657 (2005).
16. A. Bellaouchou, A. Guenbour and A. Benbachir, *Corrosion*, **49**, 656 (1993).
17. H. Iken, R. Basseguy, A. Guenbour and A. Benbachir, *Electrochim. Acta*, **52**, 2580 (2007).

18. L. Jeffus, *Welding. Principles and Applications*, p. 385, Thomson Delmar Learning, USA (1997).

19. G. F. Vander Voort, *Metallography. Principles and practice*, p. 653, ASM International, USA (1999).

20. M. T. Montañes, R. Sánchez-Tovar, J. García-Antón and V. Pérez-Herranz, *Corros. Sci.*, **51**, 2733 (2009).

21. ASTM G-61 Conducting cyclic potentiodynamic polarization measurements for localized corrosion, (2003).

22. ASTM G-5 Test method for making potentiostatic and potentiodynamic anodic polarization measurements, (2004).

23. C. Wagner and W. Traud, *Zeitschrift Fur Elektrochemie Und Angewandte Physikalische Chemie. Elektrochem*, **44**, 391 (1938).

24. G. Conde y Santiago, *Aceros inoxidables, refractarios y criogenicos*, p. 113, INTERCIENCIA, Madrid (1971).

25. G. F. Vander Voort and H. M. James, *Wrought stainless steels. Metallography and microstructure*, p. 283, ASM Handbook, USA (1992).

26. A. Neville and T. Hodgkiess, *Corros. Sci.*, **38**, 927 (1996).

27. E. McCafferty, *Corros. Sci.*, **47**, 3202 (2005).

28. M. A. Amin, S. S. bd El Rehim and H. T. M. bdel-Fatah, *Corros. Sci.*, **51**, 882 (2009).

29. E. Bardal, *Corrosion and protection. Engineering materials and processes*, p. 223, Springer, USA (2004).

30. R. G. Kelly, J. R. Scully, D. W. Shoesmith and R. G. Buchheit, *Electrochemical Techniques in Corrosion Science and Engineering*, p. 45, Marcel Dekker, New York (2003).

31. E. Otero Huerta, *Corrosión y degradación de materiales*, p. 98, Síntesis, Madrid (1997).

32. F. Mansfeld and J. V. Kendel, Laboratory studies of galvanic corrosion of aluminium alloys, Galvanic and pitting Corrosion-Field and Laboratory Studies ASTM STP 576, ASTM (1976).

33. F. T. Cheng, K. H. Lo and H. C. Man, *Surf. Coat. Tech.*, **172**, 316 (2003).

34. P. W. Atkins, *Físico Química*, Addison-Wesley Iberoamericana, Argentina (1991).

35. L. F. Garfias-Mesias and J. M. Sykes, *Corros. Sci.*, **41**, 959 (1999).

36. N. J. Laycock, *Corrosion*, **55**, 590 (1999).

37. A. Pardo, E. Otero, M. C. Merino, M. D. López, M. V. Utrilla and F. Moreno, *Corrosion*, **56**, 411 (2000).

38. M. R. El Sherif, M. I. Khaled and A. B. Waheed, *Electrochim. Acta*, **49**, 5139 (2004).

39. G. T. Burstein, C. Liu and R. M. Souto, *Biomaterials*, **26**, 245 (2005).

40. F. J. Botana, A. Aballe and M. Marcos, *Ruido Electroquímico. Métodos de análisis*, p. 22, Septem Ediciones, Oviedo (2002).

41. C. Lavos-Valereto, I. Costa and S. Wolynec, *J. Biomed. Mater. Res.*, **63**, 664 (2002).

42. S. Luiz de Assis, S. Wolynec and I. Costa, *Electrochim. Acta*, **51**, 1815 (2006).